Engineering the Microenvironment of Electron Transport Layer with Nickel Single-Atom Site for Boosting Photoelectrochemical Performance

Ying Qin [a] , Rong Tan [a] , Jing Wen [b] , Qikang Huang [c] , Hengjia Wang [a] , Mingwang Liu [a] , Jinli Li [a] , Canglong Wang [d] , Yan Shen [c] , Liuyong Hu [b, *] , Wenling Gu [a, *] , and Chengzhou Zhu [a, *]

[a] National Key Laboratory of Green Pesticide, International Joint Research Center for Intelligent Biosensing Technology and Health, College of Chemistry, Central China Normal University, Wuhan 430079, China

[b] Hubei Key Laboratory of Plasma Chemistry and Advanced Materials, School of Materials Science and Engineering, Wuhan Institute of Technology, Wuhan 430205, China

[c] Wuhan National Laboratory for Optoelectronics, Huazhong University of Science and Technology, Wuhan 430074, China

[d] Institute of Modern Physics, Chinese Academy of Science, Lanzhou 730000, China

*Corresponding author.

E-mail: huly@wit.edu.cn (Liuyong Hu);

E-mail: wlgu@ccnu.edu.cn (Wenling Gu);

E-mail: czzhu@ccnu.edu.cn (Chengzhou Zhu)

1. Experimental Procedures

Apparatus. X-ray diffraction (XRD) characterization was carried out by a D8 ADVANCE (Bruker, Germany). Transmission electron microscope (TEM) images were acquired from a Titan G260-300 (Thermo Fisher, United States). The aberration-corrected high-angle annular dark-field scanning transmission electron microscopy (AC-HAADF-STEM) was carried out on was performed by a Titan G2-600 (FEI, Unites States). Ultraviolet photoelectron spectroscopy (UPS) measurements were performed on a Thermo Scientific ESCALAB Xi+ with an Al Kα X-ray source and monochromatic He I radiation (21.22 eV), respectively. The Ultraviolet-visible (UV-Vis) diffuse-reflectance absorption spectra were measured on a UV-Vis spectrophotometer (Agilent Technologies, Cary 100) using $BaSO_4$ as reflectance standard reference. Electrochemical impedance spectroscopy (EIS), Mott-Schottky (M-S) curve and the activity of oxygen reduction reaction (ORR) test were performed on a CHI660E electrochemical workstation (Shanghai Chenhua Apparatus Corporation, China) with a three-electrode system. Photoelectrochemical test was performed on a system containing a CHI842d electrochemical workstation (Shanghai Chenhua Instrument Co., Ltd.), 500 W Analog Daylight Xenon Light Source (PLS-FX300HU, Beijing Perfectlight Technology Co., Ltd.) with a 420 nm cut-off filter. Electron paramagnetic resonance (EPR) measurements were carried out on EMXmicro-6/1 (Bruker, Germany). The scanning electrochemical microscopy (SECM) investigation of the interface carrier dynamics process was carried out with a CHI 920C SECM bipotentiostat.

Reagents. Nickel acetate, 1, 10-phenanthroline monohydrate, Jacobsen's ligand, and copper oxide (CuO) were purchased from Aladdin Ltd. (Shanghai China). Potassium dihydrogen phosphate (KH_2PO_4), and dipotassium hydrogen phosphate (K_2HPO_4) were obtained from Sinopharm

Chemical Reagent Co., Ltd (Shanghai, China). Paraoxon was bought from Dr. Ehrenstorfer GmbH (Augsburg, Germany). Acetylthiocholine (ATCh) and acetylcholinesterase (AChE) were purchased from Sigma-Aldrich. The 96-well plates were purchased from Thermo Fisher Scientific Inc. Indium-tin oxide coated glass (ITO, 10 Ω, 1.1 mm) was ordered from Foshan Yuanjingmei Glass Co., Ltd. Unless stated, all the chemicals mentioned above were analytical reagents and used as received. The deionized water in all experiments was prepared in a three-stage Millipore Milli-Q plus 185 purification system and with a resistivity higher than 18.2 MΩ*cm.

Synthesis of Ni-N_4@C. 1, 10-phenanthroline monohydrate (29.7 mg), Nickel acetate (12.4 mg) and 2 mL ethanol were mixed and stirred for 20 minutes to form a transparent solution at 60 ℃. The solution was then added with carbon black (69.6 mg), and the resulting dispersion was heated at 60 ℃ for 4 hours under continuous magnetic agitation. They were then centrifuged with ethanol and dried at 80 ℃. The resulting black powder was transferred to a ceramic crucible and heated to 600℃ in a tubular furnace with a rate of 10 ℃ min^{-1} for 2 h under an atmosphere of N_2. And the product was treated in 30% acetic acid solution (40 mL) for 2 h to remove any residual ligand. The product was then washed with water and ethanol and dried.

Synthesis of Ni-N_2O_2@C. Nickel acetate (14.8 mg) was added into 5 mL ethanol and stirred for 10 min to form a transparent solution. Then (R,R)-(-)-N,N'-bis(3,5-di-tert-butylsalicylidene)-1,2-cyclohexanediamine (Jacobsen's ligand, 292.2 mg) was added to the above nickel acetate solution, and stirred and heated continuously in an oil-bath at 60℃ for 4 h. Subsequently, carbon black (69.6 mg) was added to the solution and heated at 60 ℃ for 4 h. They were then centrifuged with ethanol and dried at 80 ℃. The resulting powder was lightly ground in a mortar and pestle and transferred to a ceramic crucible, heated to 300 ℃ in a tubular furnace with a rate of 10 ℃ min^{-1} under an

atmosphere of N_2, and then kept at 300 ℃ for 2 h. After natural cooling to room temperature, the product was treated in 30% acetic acid solution (40 mL) for 2 h to remove any residual Jacobsen ligand.

Fabrication of Photoelectrode. CuO and Ni-N_4@C were assembled by electrostatic adsorption. Ni-N_4@C was dispersed in deionized water (2 mg/mL) with ultrasonic treatment for 40 min. Next, Ni-N_4@C/CuO with 7.4% Ni-N_4@C (the optimal ratio) loading amount was obtained by the formula in Table S2. They were mixed with ultrasonic treatment for 30 min and then implemented on a shaker for 1 h. Ni-N_4@C/CuO with inequable Ni-N_4@C load was gained by regulating the mass of Ni-N_4@C in 500 μL liquid containing 7 mg CuO. Ni-N_2O_2@C/CuO (C/CuO) with 7.4% Ni-N_2O_2@C (C) loading was prepared by the same method as Ni-N_4@C/CuO with 7.4% Ni-N_4@C.

PEC Measurement System. Before electrode modification, ITO slices were ultrasonically washed with distilled water and ethanol for 30 min, respectively, and dried at 60 °C. 5 μL of the above mixture was then deposited on the ITO electrode with a circular area of ~0.28 cm^2 (diameter = 6 mm). After being baked at 60 °C in a vacuum drying oven, the materials-modified ITO electrodes were obtained. Photocurrent measurement was carried out in 0.1 M PBS (pH 7.4) buffer solution as the electrolyte with a classical three-electrode system, using a modified-ITO electrode, Pt wire, and Ag/AgCl as working electrode, counter electrode and reference electrode, respectively. A 500 W xenon lamp with a cut-off filter ($\lambda \geq 420$ nm) was used as the exciting light source and switched on and off every 10 s. The applied electrochemical method was chronoamperometry, and the external bias voltage was -0.1 V (vs. Ag/AgCl).

Electrochemical Tests. The activity of ORR was tested on a CHI660 electrochemical workstation. Specifically, a glassy carbon disc with a Pt ring electrode (RRDE, 0.56 cm in diameter or 0.2462

cm^2 in surface area; 37% theoretical collection efficiency) served as the working electrode, and platinum foil and a saturated calomel electrode were employed as the counter electrode and reference electrode, respectively. O_2-saturated 0.1 M PBS buffer solution (pH = 7.4) served as the electrolyte for ORR performance tests. Linear sweep voltammetry measurements were conducted with a rotational speed of the working electrode at 1600 rpm. On the ring, the applied voltage was at 0.5 V to collect the generated H_2O_2. Furthermore, the yield of hydrogen peroxide H_2O_2% and electron transfer number (n) were calculated using the following equation.

$$H_2O_2\% = \frac{200i_r/N}{|i_d| + i_r/N}$$

(Equation S1)

$$n = \frac{4|i_d|}{|i_d| + i_r/N}$$

(Equation S2)

where i_d is the disc current, i_r is the ring current, and N is the ring collection efficiency.

SECM Measurement System. The Pt ultramicroelectrode (UME, 25 μm), a Pt wire counter electrode and an Ag/AgCl reference electrode were fixed onto a homemade Teflon cell of 7 mL volume. The photocathode was installed at the bottom of the cell as the substrate electrode. The electrode was brought to a conical shape with an RG of 10, where RG refers to the ratio between the diameters of the glass sheath and the Pt disk. The photoexcitation was performed from the back of the photoanode with a 500 W Analog Daylight Xenon Light Source (PLS-FX300HU, Beijing Perfect light Technology Co., Ltd.).

SECM Data Fitting. The approach curves on the UME (I_T-L curve) were fitted by an analytical function of the approach curve for an insulating substrate and a conductive substrate proposed by

Lefrou and Cornut.[1-2]

For insulating substrate,

$$I_T^{ins}(L,RG) = \frac{\left(\frac{2.08}{RG^{0.358}}\right)\left(L - \left(\frac{0.145}{RG}\right)\right) + 1.585}{\left(\frac{2.08}{RG^{0.358}}\right)(L + 0.00238RG) + 1.57 + \left(\ln\frac{RG}{L}\right) + (2/\pi RG)\ln\left(1 + \left(\frac{\pi RG}{2L}\right)\right)}$$

(Equation S3)

For conductive substrate,

$$I_T^{cond}(L + \kappa,RG) = \alpha(RG) + \frac{\pi}{4\beta(RG)\arctan(L + \kappa)} + \left(1 - \alpha(RG) - \frac{1}{2\beta(RG)\pi}\frac{2}{\arctan(L + \kappa)}\right)$$

(Equation S4)

$$\alpha(RG) = \ln 2 + \ln 2\left(1 - \frac{2}{\pi}\arccos\left(\frac{1}{RG}\right)\right) - \ln 2\left(1 - \left(\frac{2}{\pi}\arccos\left(\frac{1}{RG}\right)\right)^2\right)$$

(Equation S5)

$$\beta(RG) = 1 + 0.639\left(1 - \frac{2}{\pi}\arccos\left(\frac{1}{RG}\right)\right) - 0.186\left(1 - \left(\frac{2}{\pi}\arccos\left(\frac{1}{RG}\right)\right)^2\right)$$

(Equation S6)

For actual substrate,

$$I_T(L,RG,\kappa) = I_T^{cond}\left(L + \frac{1}{\kappa},RG\right) + \frac{I_T^{ins}(L,RG) - 1}{(1 + 2.47RG^{0.31}L\kappa)\left(1 + L^{0.006RG + 0.1}13\kappa^{-0.023RG + 0.91}\right)}$$

(Equation S7)

$$k_{eff} = \kappa D/r_T$$

(Equation S8)

where, I_T^{ins} describes the current if no reaction occurs at the insulating sample ("negative feedback"), I_T^{cond} is the diffusion-controlled mediator recycling at the sample ("positive feedback"), κ is the apparent charge transfer rate constant of the substrate, k_{eff} is the effective charge transfer rate

constant of the substrate, and D is the diffusion coefficient of the electroactive substance in the solution.

Detection of Organophosphorus Pesticides. AChE (100 μL) with the activity of 500 mU/mL were first incubated with different concentrations of paraoxon (100 μL) from 0.03 ng/mL to 50 ng/mL for 15 minutes at 37 °C. Then, 1 mM acetylthiocholine (25 μL) was added above the solution for 40 minutes at 37 °C. Next, the electrodes were soaked in the above solution at room temperature for 15 minutes.

Organophosphorus Pesticides Detection in Real Samples. The proposed PEC strategy was used for paraoxon detection in agricultural samples, including cucumber, tomato, apple, and cabbage. These samples were purchased from a local market. These samples were immersed in paraoxon standards of 200 ppm for 15 min. The surface of the sample is then tested for residual pesticides by using gas chromatography (GC). (1) The residual pesticide was dissolved with 2.0 mL n-hexane and detected by using GC. Afterward, the quantified actual samples were diluted to obtain different concentrations of residual pesticides for the determination of recovery. (2) The diluted residual pesticide was dissolved with PBS buffer (0.1 M, pH = 7.4), and paraoxon concentration in the real sample was detected by using the current method based on the calibration curve.

Computational Methods. The theoretical calculations are carried out using the Density Functional Theory (DFT) based plane wave pseudo-potential approach. All calculations were done on the Materials Studio platform. CASTEP (Cambridge Serial Total Energy Package) module was used by an approximation Generalized gradient approximation (GGA) and a Perdew, Burke and Emzerhof (PBE). To have the preferred effect in these samples, 2 × 3 supercell is built. A reasonable vacuum region was set around 22 Å in the vertical direction to avoid interaction between planes. For

CASTEP calculation, total energy dependence on the energy cut off was 600 eV. For making certain the factors of convergence for the energy calculation and geometry optimization, 4 × 4 × 1 k-points have been utilized for samples.

2. Supporting Figures

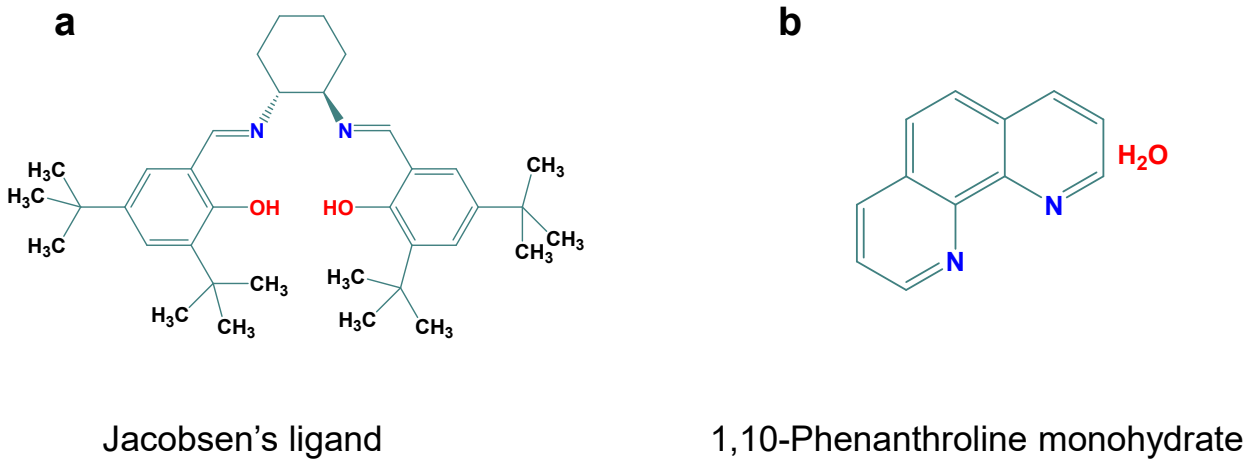

Fig. S1. Ligand molecular formula for synthesis of (a) Ni-N_2O_2@C and (b) Ni-N_4@C.

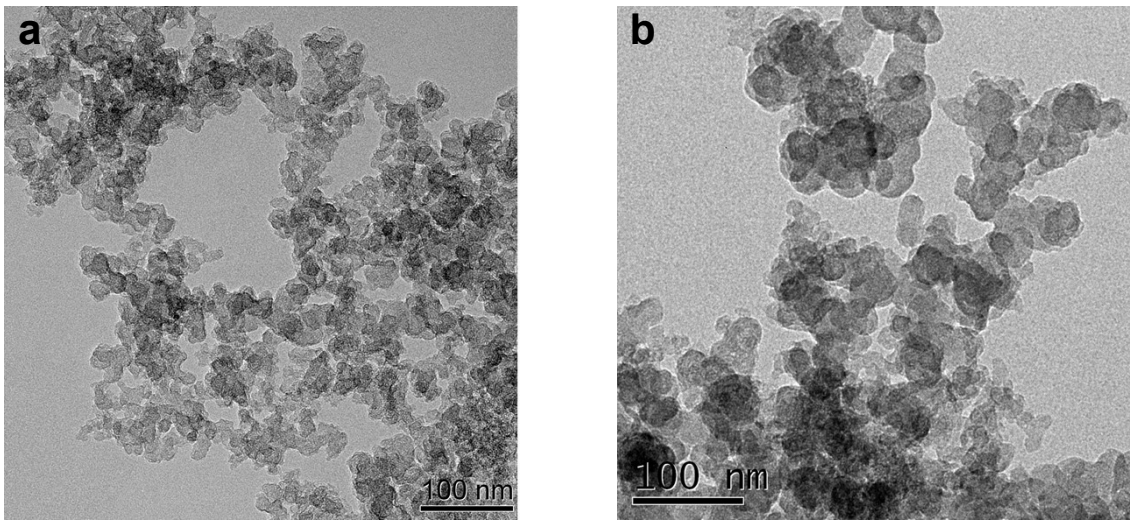

Fig. S2. TEM images of (a) Ni-N_4@C and (b) Ni-N_2O_2@C.

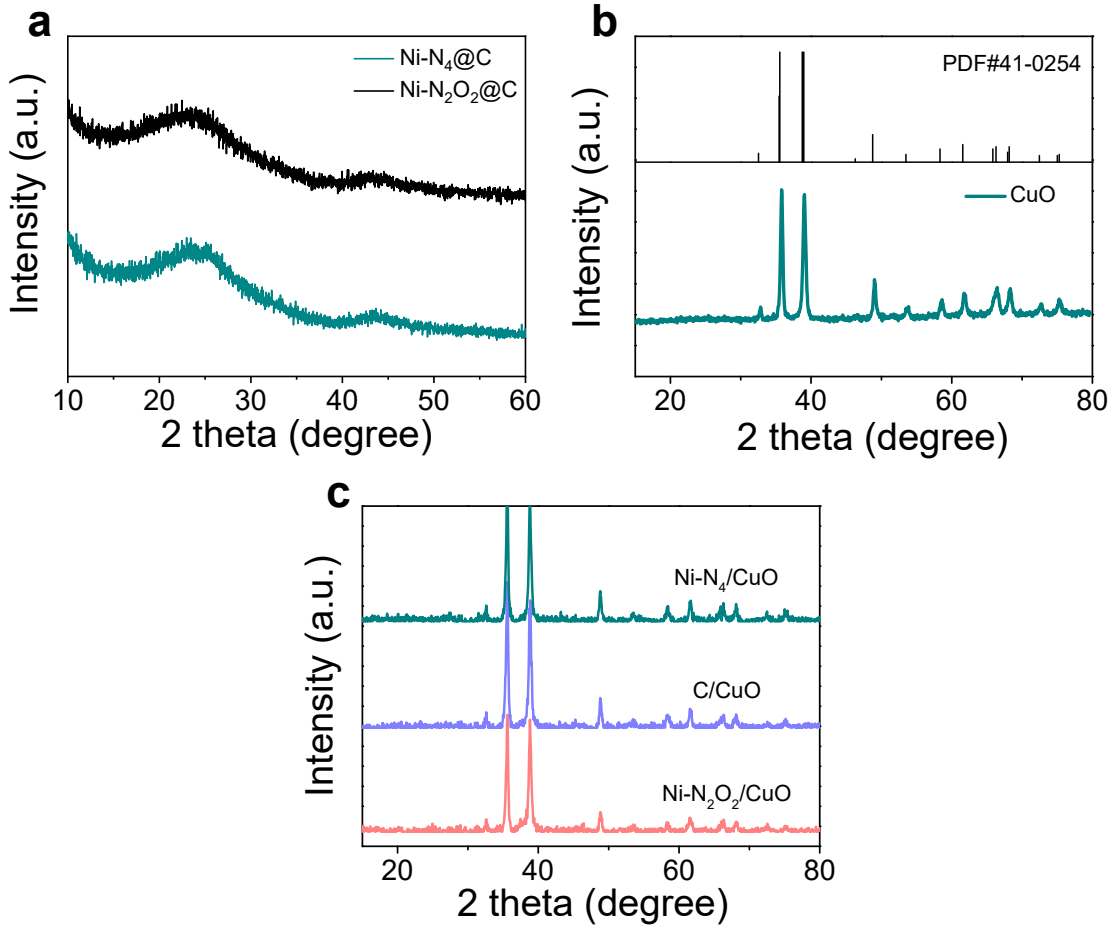

Fig. S3. (a) XRD of Ni-N_4@C and Ni-N_2O_2@C. (b) XRD of CuO. (c) XRD of Ni-N_4@C/CuO, C/CuO, Ni-N_2O_2@C/CuO.

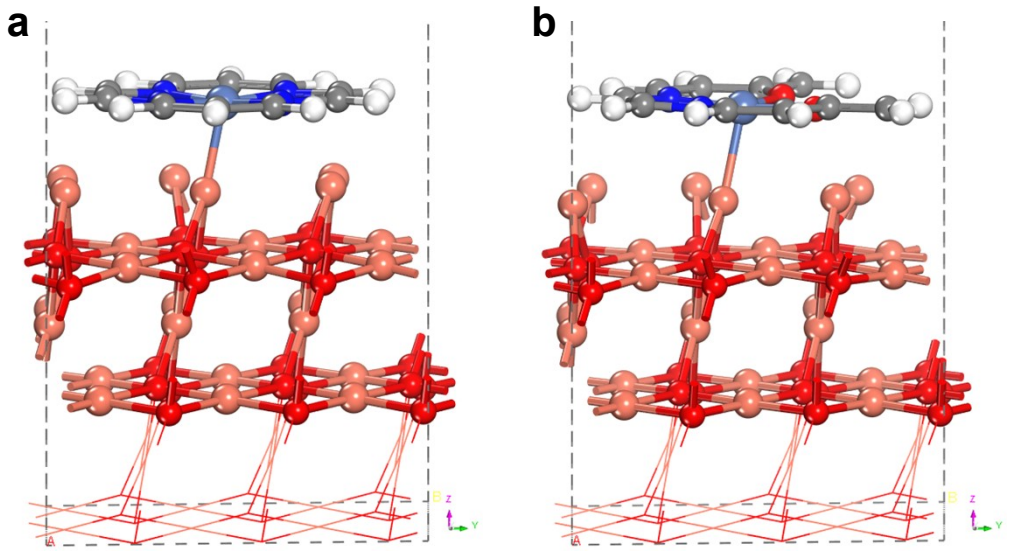

Fig. S4. Optimized geometric structures of (a) Ni-N_4@C/CuO(110) and (b) Ni-N_2O_2@C/CuO(110).

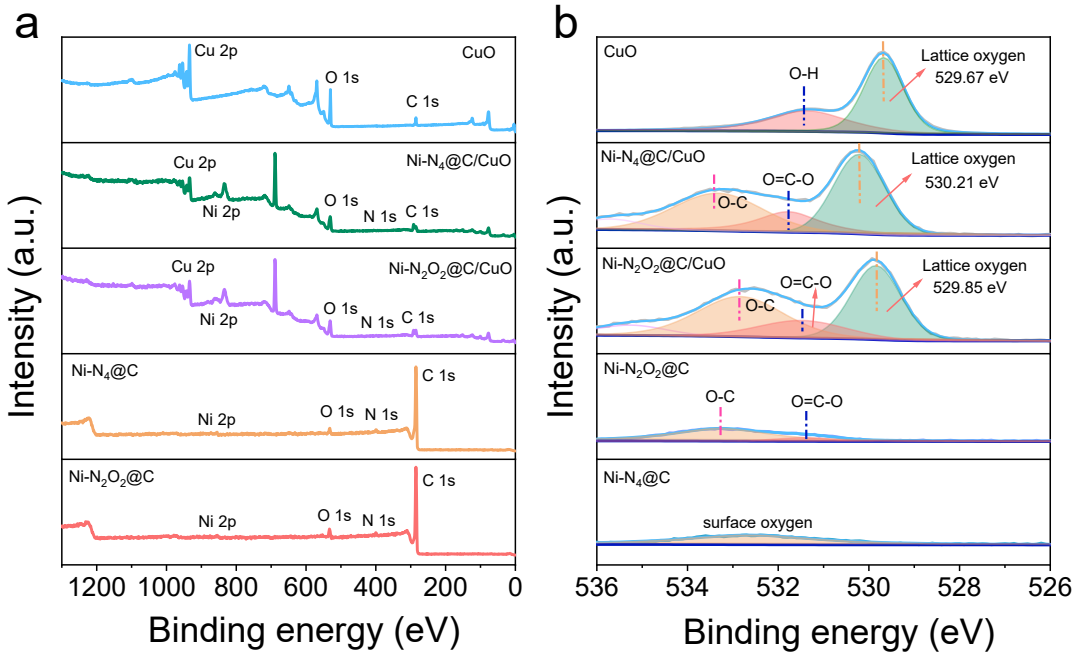

Fig. S5 (a) XPS survey and (b) high-resolution O 1s XPS spectrum of CuO, Ni-N_4@C, Ni-N_2O_2@C, Ni-N_4@C/CuO, and Ni-N_2O_2@C/CuO.

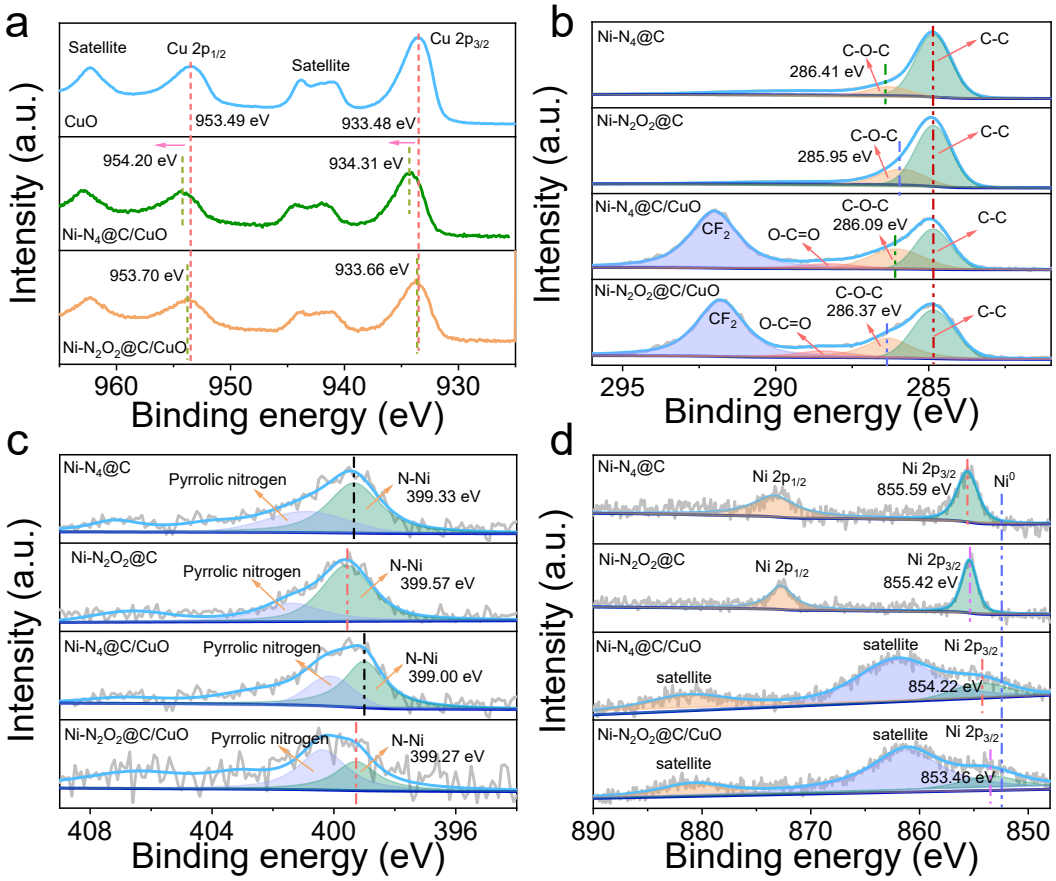

Fig. S6 (a) High-resolution Cu 2p XPS of CuO, Ni-N_2O_2@C/CuO and Ni-N_4@C/CuO. High-resolution (b) C 1s, (c) N 1s and (d) Ni 2p XPS of Ni-N_4@C, Ni-N_2O_2@C, Ni-N_2O_2@C/CuO and Ni-N_4@C/CuO.

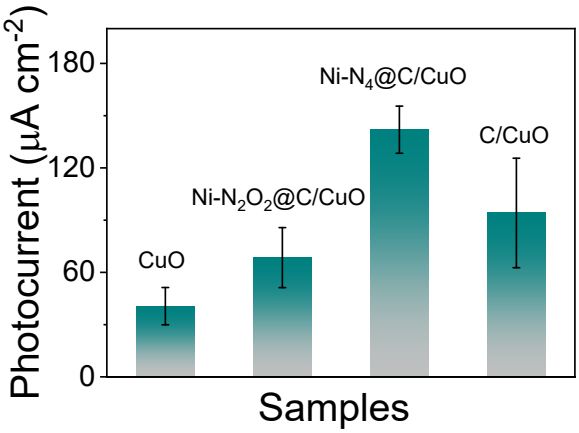

Fig. S7. Photocurrent responses for CuO, Ni-N_2O_2@C/CuO, C/CuO, Ni-N_4@C/CuO.

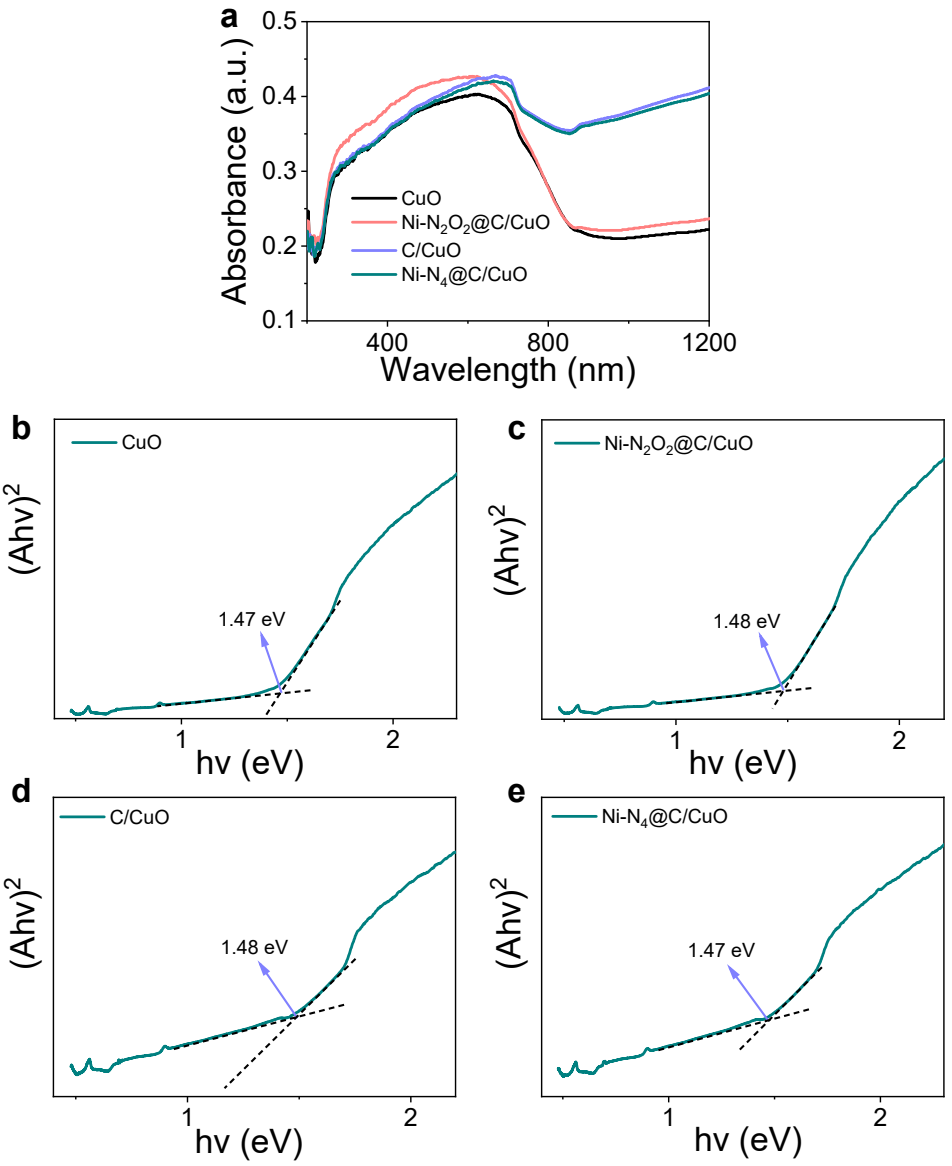

Fig. S8. (a) UV-vis diffuse-reflectance spectra of CuO, Ni-N_2O_2@C/CuO, C/CuO and Ni-N_4@C/CuO. Tauc plot of (b) CuO, (c) Ni-N_2O_2@C/CuO, (d) C/CuO and (e) Ni-N_4@C/CuO.

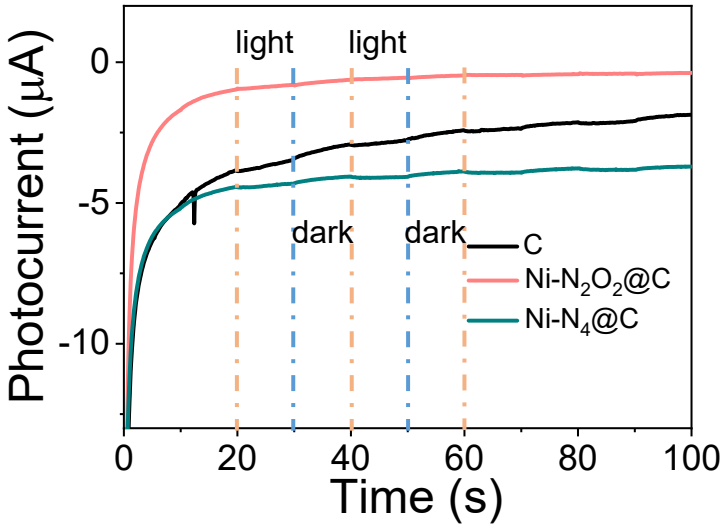

Fig. S9. Photocurrent responses for C, Ni-N_2O_2@C and Ni-N_4@C.

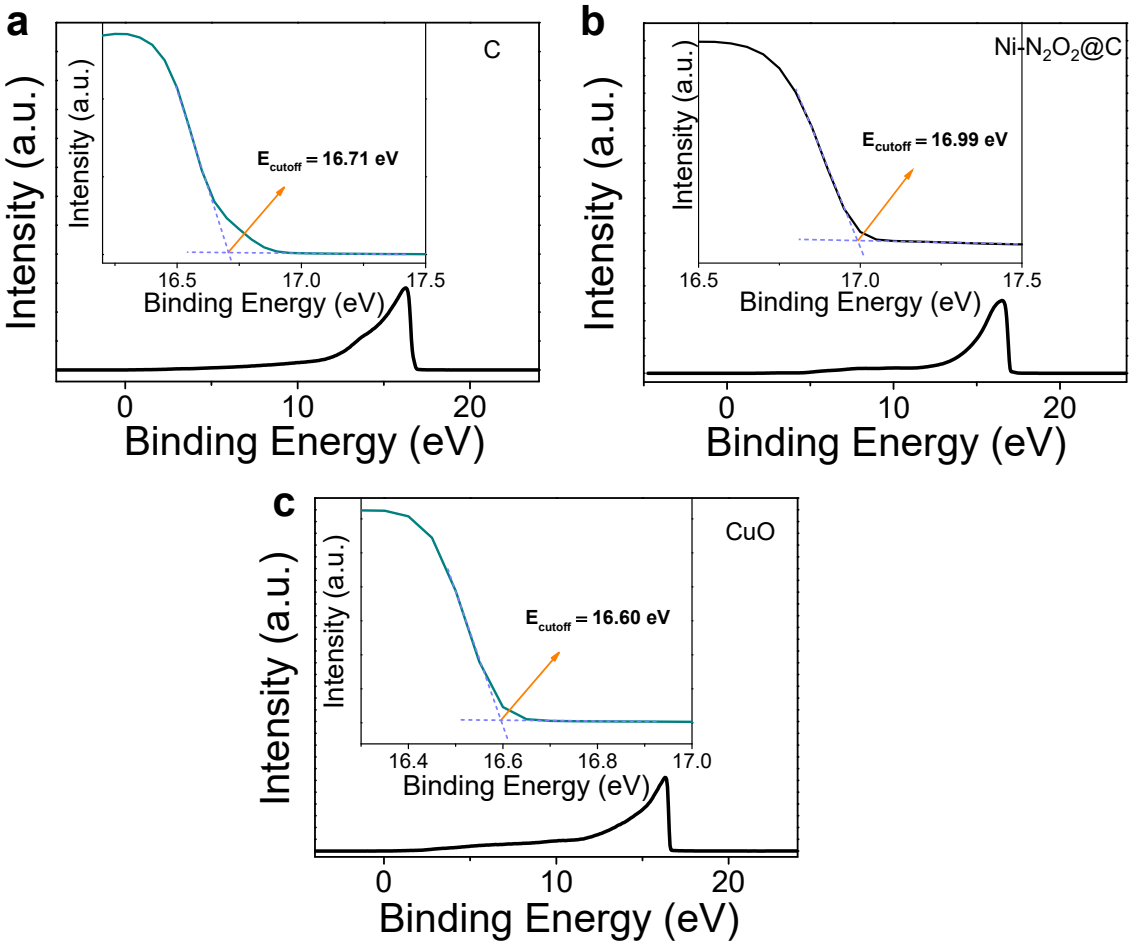

Fig. S10. UPS of (a) C, (b) Ni-N_2O_2@C and (c) CuO.

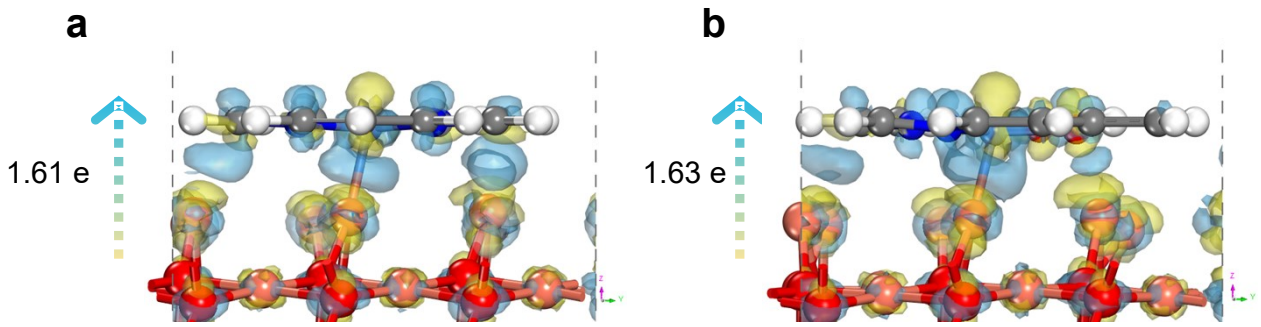

Fig. S11. Side view of the charge density difference for (a) Ni-N_4@C/CuO and (b) Ni-N_2O_2@C/CuO. The transferred electron was determined by Mülliken charge calculations. The blue and yellow iso-surfaces depict charge accumulation and depletion in the space, respectively.

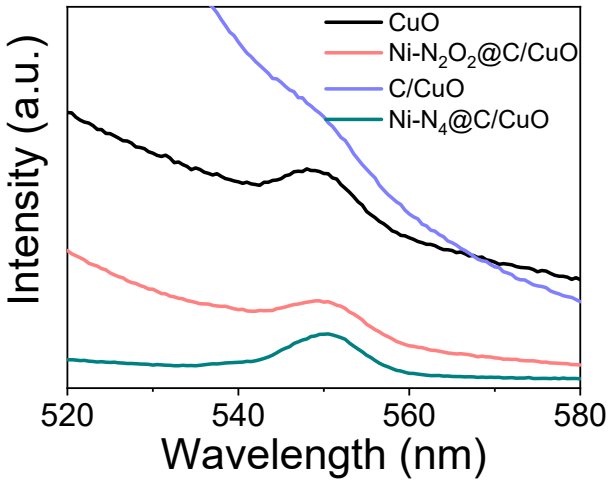

Fig. S12. Steady-state photoluminescence spectra of CuO, Ni-N_2O_2@C/CuO, C/CuO and Ni-N_4@C/CuO.

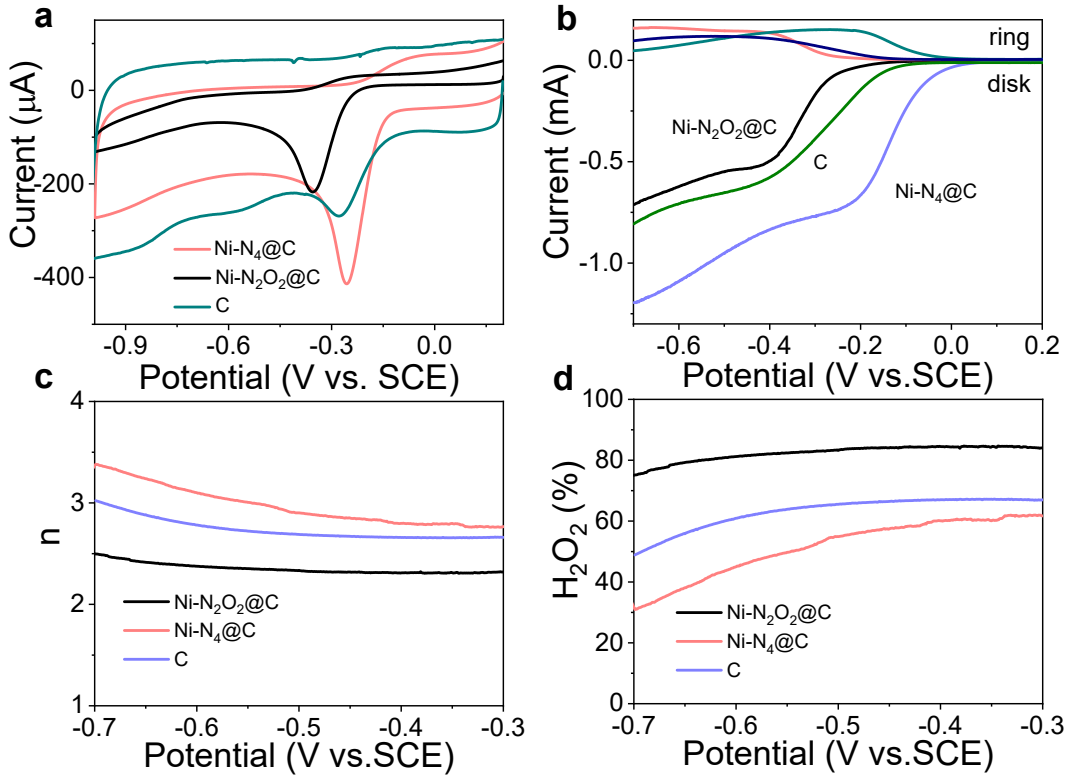

Fig. S13. (a) CV curves of Ni-N_4@C, Ni-N_2O_2@C and C in O_2-saturated 0.1 M PBS buffer solution (pH = 7.4) at 10 mV/s. (b) RRDE polarization curves of Ni-N_2O_2@C, Ni-N_4@C and C at 1600 rpm in O_2-saturated 0.1 M PBS buffer solution (pH = 7.4) with the ring current and disk current. (c) Average electron transfer number and (d) H_2O_2 selectivity (%) during the ORR tests of Ni-N_4@C, Ni-N_2O_2@C and C.

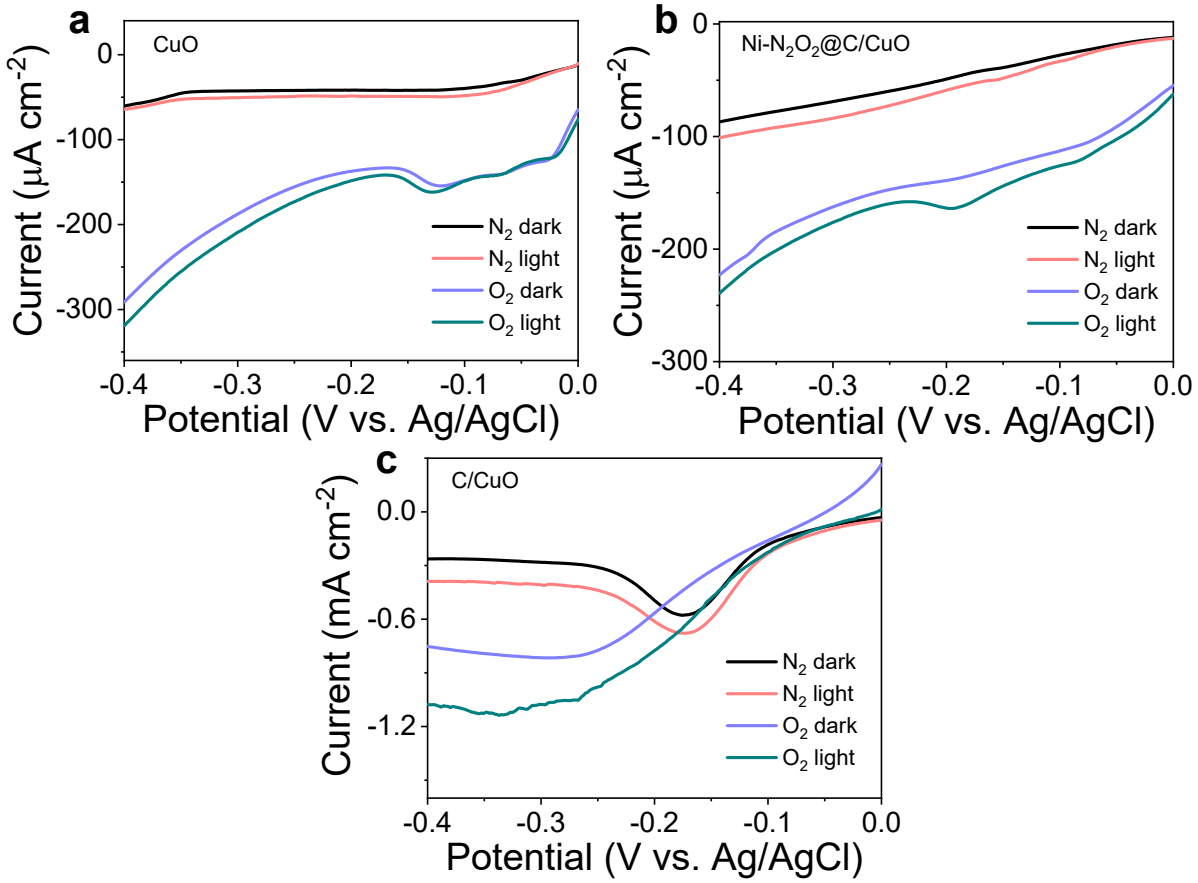

Fig. S14. LSV (with and without light) of (a) Ni-N_4@C/CuO, (b) Ni-N_2O_2@C/CuO and (c) C/CuO in the O_2 and N_2 saturated-buffer electrolyte, respectively.

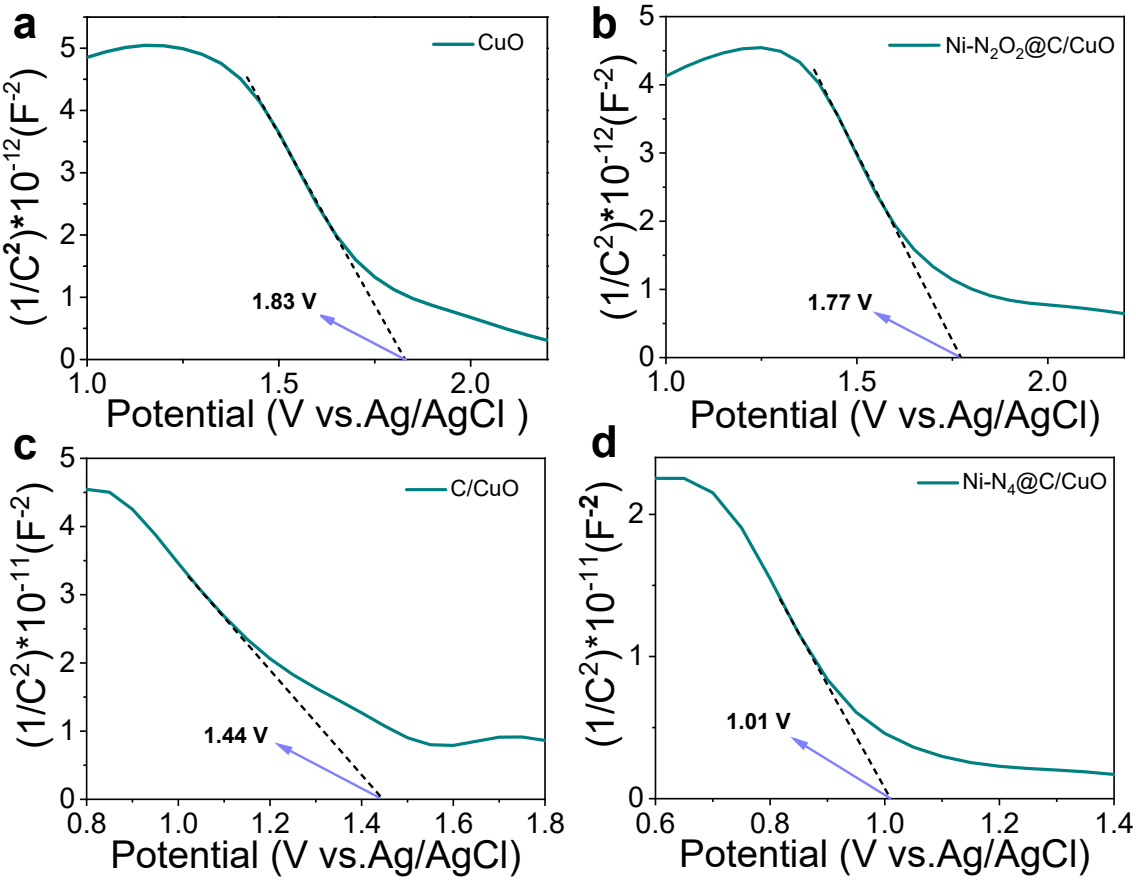

Fig. S15. Mott-Schottky plots for (a) CuO, (b) Ni-N_2O_2@C/CuO, (c) C/CuO and (d) Ni-N_4@C/CuO at the selected frequency of 1000 Hz.

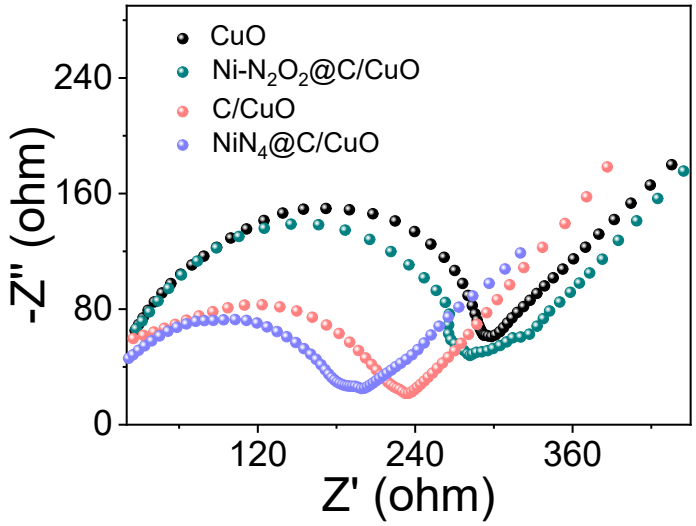

Fig. S16. EIS for CuO, Ni-N_4@C/CuO, Ni-N_2O_2@C/CuO and C/CuO.

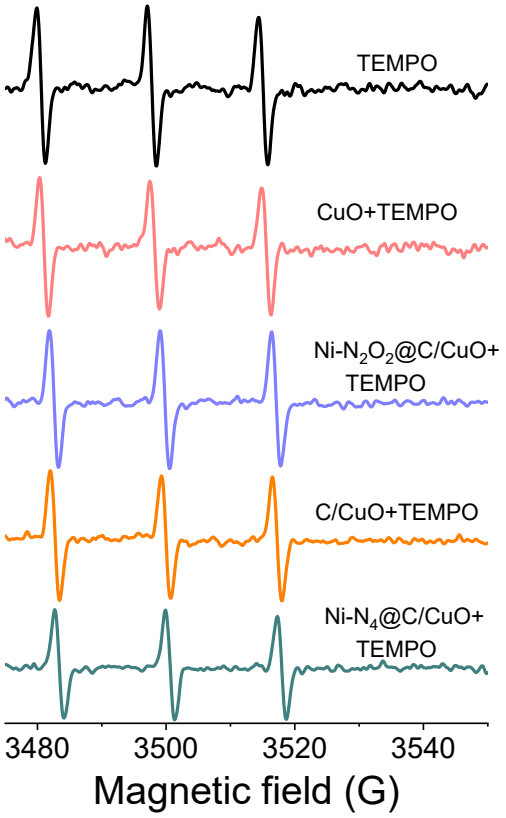

Fig. S17. EPR spectra obtained at room temperature from samples containing 0.03 mM TEMPO in the absence (control) and presence of CuO, Ni-N_2O_2@C/CuO, C/CuO, Ni-N_4@C/CuO without irradiation.

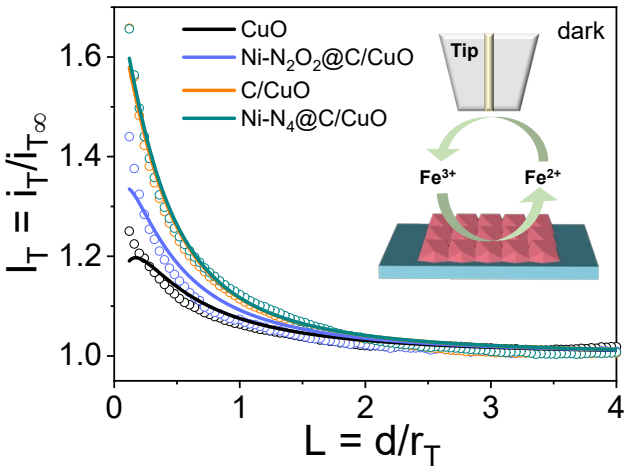

Fig. S18. Normalized SECM approach curves in the feedback mode with the Pt UME approaching different samples with the redox mediator 2 mM $[Fe(CN)_6]^{4-}$ under dark, r_T = 12.5 μm.

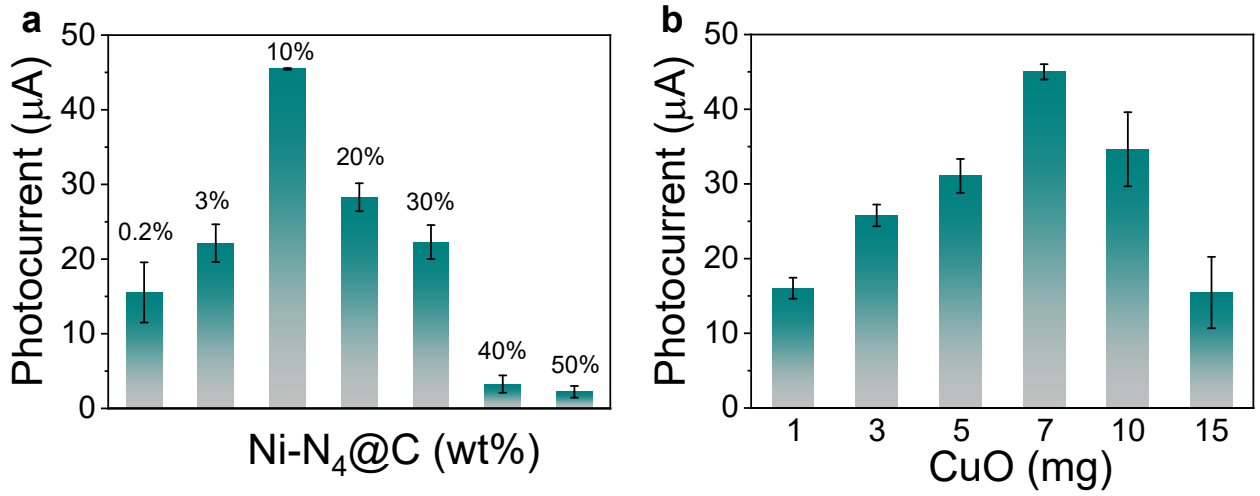

Fig. S19. Optimization of the loading of (a) Ni-N_4@C and (b) CuO.

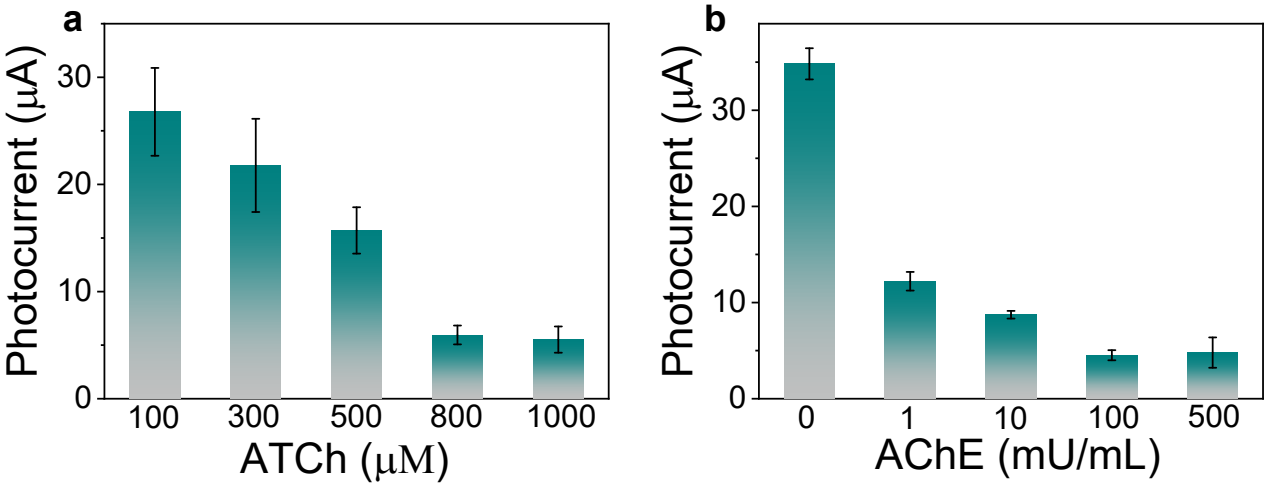

Fig. S20. Optimization of the concentration of (a) ATCh and (b) AChE.

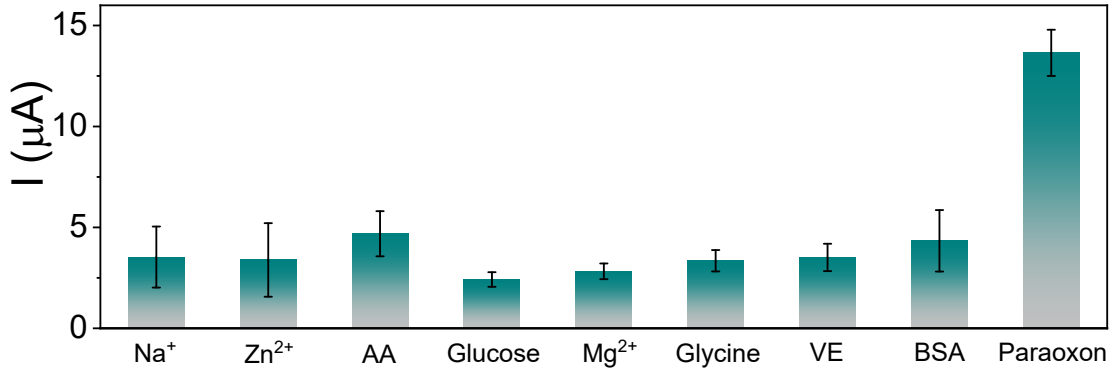

Fig. S21. Selectivity of the proposed biosensor.

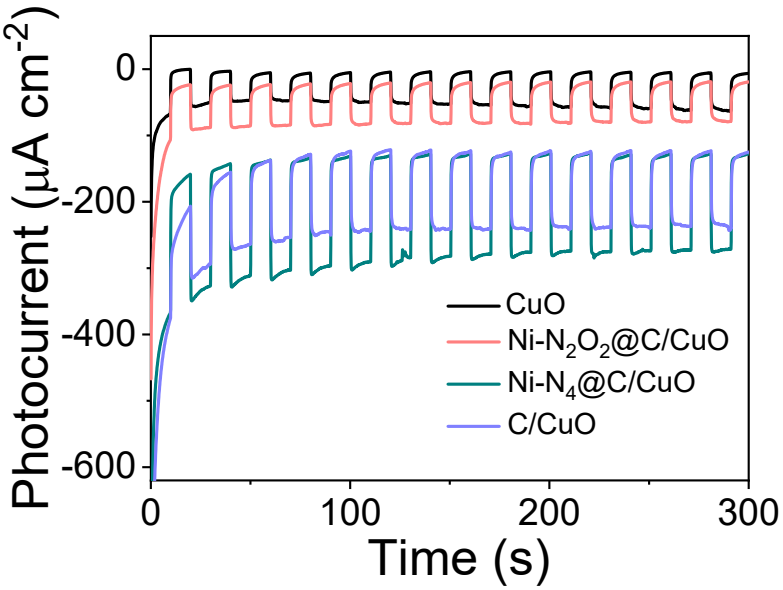

Fig. S22. Stability with different samples.

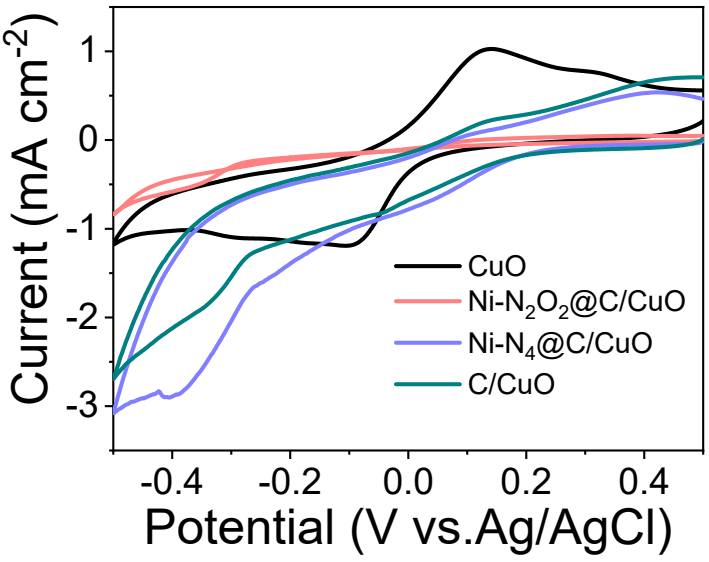

Fig. S23. CV of CuO, Ni-N_4@C/CuO, Ni-N_2O_2@C/CuO and C/CuO in the air saturated-buffer electrolyte under illumination.

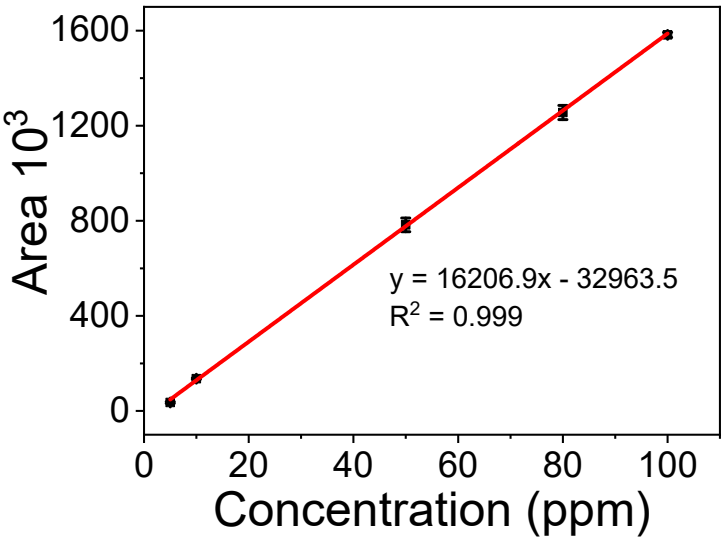

Fig. S24. Gas chromatographic standard curve of paraoxon at different concentrations.

Table S1. The fitting result of charge transfer rate constant κ.

Samples	κ_{dark}	κ_{light}
CuO	1.60	1.85
Ni-N_2O_2@C/CuO	1.88	2.18
C/CuO	2.40	2.99
Ni-N_4@C/CuO	2.43	5.52

Table S2. Formula of Ni-N_4@C/CuO with 7.4% Ni-N_4@C loading amounts.

	CuO	**Ni-N_4@C (2 mg/mL)**	**DI water**	**Ethanol**	**0.5% Nafion**
7.4%	7 mg	280 μL	10 μL	200 μL	10 μL

Table S3. Recovery rates of the Ni-N_4@C/CuO-based PEC sensor for paraoxon detection.

	Added Concentration (ng/mL)	**Founded concentration (ng/mL)**	**Recovery (%)**	**RSD (%, n=3)**
cucumber	10	10.12	101.2	7.25
	3	2.89	96.33	4.23
tomato	2	2.16	108.0	3.29
	40	40.02	100.1	6.74
apple	7	6.95	99.29	1.56
	10	10.14	101.4	3.25
cabbage	0.1	0.09	90.00	4.76
	10	11.05	110.5	6.65

(1) Cornut, R.; Lefrou, C., New analytical approximation of feedback approach curves with a microdisk SECM tip and irreversible kinetic reaction at the substrate. *J. Electroanal. Chem.* **2008,** *621*, 178-184.

(2) Lefrou, C.; Cornut, R., Analytical expressions for quantitative scanning electrochemical microscopy (SECM). *ChemPhysChem* **2010,** *11*, 547-556.